NOVEL ABSORBER MEMBRANE AND THERMOCOUPLE DESIGNS FOR CMOS-MEMS THERMOELECTRIC INFRARED SENSOR

Kai-Chieh Chang [1], Ya-Chu Lee [1], Chih-Ming Sun [3], and Weileun Fang [1,2]
[1]Dept. of Power Mechanical Engineering, National Tsing Hua University, Hsinchu, Taiwan
[2]Institute of NanoEngineering and MicroSystems, National Tsing Hua University, Hsinchu, Taiwan
[3]PixArt Imaging Inc., Hsinchu Science Park, Hsinchu, Taiwan

ABSTRACT

This study designs and implements a thermoelectric IR sensor using TSMC 0.35μm 2P4M standard CMOS process. The novel design has three major concerns: heat conduction of the absorber membrane, distribution of the thermocouple, and etching release holes for post-CMOS process. Proposed design significantly increase the thermal resistance and responsivity of IR sensor. As compare with the reference design, the presented design could increase the responsivity for 6-fold at 25mtorr working pressure.

Keywords: CMOS-MEMS; thermoelectric; infrared sensor; thermopile

INTRODUCTION

Recently, infrared sensors are well developed and have lots of applications in various areas such as non-contact temperature measurement, night vision and human behavior detection, etc. Uncooled IR detectors including bolometer, pyroelectric and thermoelectric sensor could convert the generated heat from absorbed incoming photons to a detectable electrical signal [1]. The sensing mechanism of thermoelectric sensor is based on the Seebeck effect to transfer heat to voltage. In general, as compare with the bolometer, the thermoelectric sensor has lower noise but poor sensitive. Thermoelectric infrared sensor implemented using single spiral absorber [2], multi-layer stacking [3], stand-alone structure [4] have been demonstrated. The CMOS processes have been exploited for IR detectors [5-7], yet an additional metal-black coating film is required [6]. To further meet the requirements for applications, smaller size and higher responsivity become two important design specifications for the development of the thermoelectric infrared sensor. Moreover, the vacuum package is also employed to enhance the performance. Nevertheless, there are plenty of room for the designs of absorber membrane and thermocouple using the multi-layer CMOS process.

DESIGN CONCEPT

Based on the standard CMOS process, this study presents a thermoelectric infrared sensor with structure and thermocouple (TC) designed for high responsivity when operating at low pressure (Fig. 1a). The reference design in Fig. 1b is used for comparison. In general, the etching release holes are designed based on the required process time to suspend MEMS structures. However, in this study, the etching release holes may affect the heat transfer path and also the distribution of TCs for the thermoelectric infrared sensor. In Fig. 1a, the proposed IR sensor design with a novel absorber membrane exhibits a suspended structure with strip-via releasing holes split the absorber membrane into serpentine shape to enhance the thermal resistance. Moreover, the serpentine design can extend the length of TC and further increase its temperature difference between two ends. The dielectric material has great ability for the absorption of infrared radiation. Hence, CMOS dielectric layers are employed to form the suspended membrane, and the serpentine TCs are designed to embed in the membrane.

In comparison, the IR sensor consisting of absorber membrane with typical discrete releasing holes is also designed in Fig. 1b. Thus the number and distribution of TCs are different with the design in Fig. 1a. To make a fair comparison, these two designs had the same membrane dimension and thickness. Note the TC consists of two poly layers which have different doping concentration in TSMC 0.35 μm 2P4M standard CMOS process. These two poly

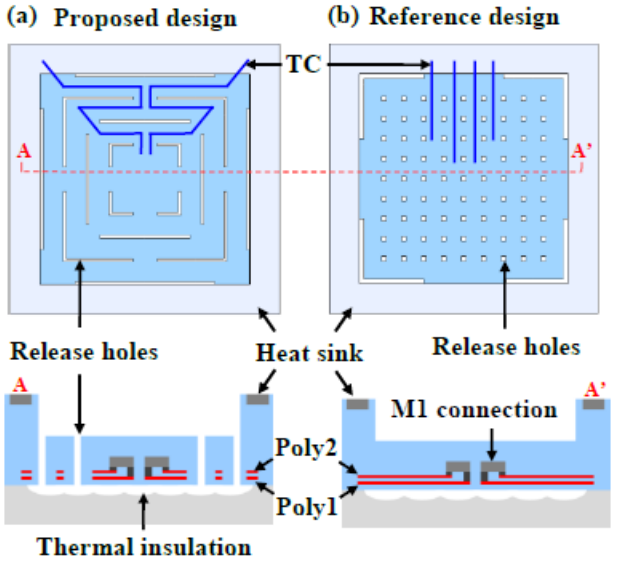

Figure 1: Design concept of infrared sensor, (a) proposed design for membrane, thermocouples, and release holes, and (b) reference design.

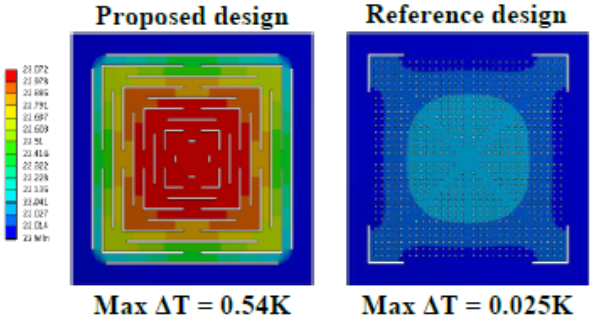

Figure 2: Simulation of temperature distribution and variation for the proposed and reference designs.

layers are connected by metal1 and patterned along with the absorber membrane. The resistance of TCs will influence the noise level. Therefore, to make a fair comparison between the two designs in Fig. 1, their TCs are designed to have the same resistance.

Fig. 2 shows the typical temperature distribution predicted by the finite element software. As indicated by the color bars, the temperature difference ΔT is increased for near 20-fold for the proposed suspended structure design, and the distribution of TC (depicted in Fig. 1a) is along the temperature gradient.

FABRICATION PROCESS AND RESULT

Fig. 3 shows the process steps to fabricate the CMOS-MEMS infrared sensor. Fig. 3a shows the multi-layer stacking and patterning after chip out from TSMC 0.35μm 2P4M (2-poly, 4-metal) standard CMOS process. Fig. 3b shows the post-CMOS process metal wet etching by H_2SO_4/H_2O_2 that was used to etch metal and tungsten-via to define the absorber membrane. Fig. 3c shows reactive-ion etching used to open the pads for wire bonding. Fig. 3d shows the Xenon difluoride Si etching to suspend the structure for the prevention of heat transfer by thermal conduction from the silicon substrate. Finally the MEMS chip was wire-bonded on PCB for testing.

The SEM micrographs in Fig. 4a, and 4c respectively show the typical fabricated chips including proposed design with strip-via holes and reference design with discrete releasing holes. The structure deformation caused by residual stress is suppressed by the fixed boundary

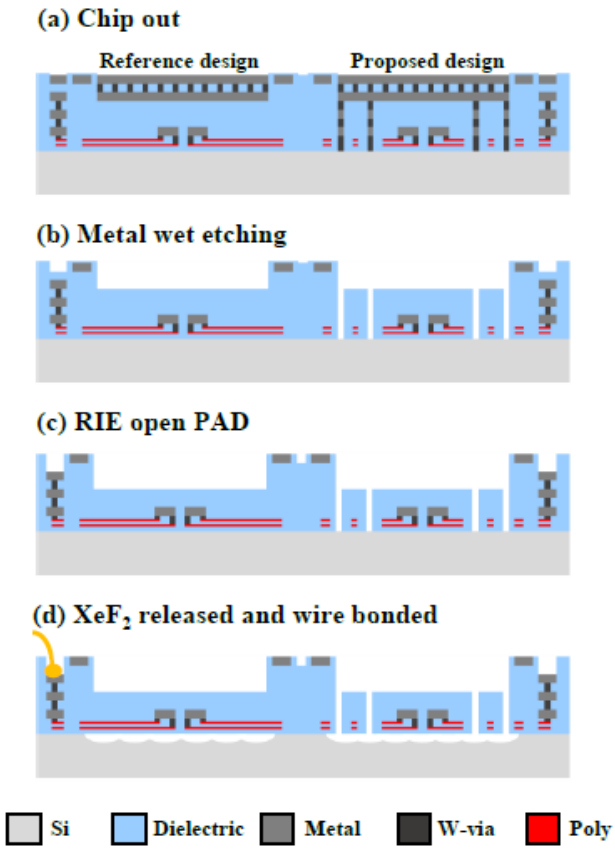

Figure 3: Process steps, (a) chip prepared by TSMC, (b-d) post-CMOS process to pattern and release structures.

design. The optical micrographs in Fig. 4b, and 4d respectively show the two poly stacking structure as TCs embedded in the absorber membrane. Note that the width of poly2 layer is smaller than poly1 layer by following the design rule of CMOS process.

MEASUREMENT SETUP AND RESULT

As in Fig. 5, the test setup includes an external sensing circuit on PCB with amplifier, low pass filter, and one commercial reference. After that, the fabricated chip was wire-bonded in a ceramic house and then covered with a Si optical filter in order to block visible light. The packaged chip and its sensing circuit were mounted on a PCB for testing, and a commercial IR sensor is used as a reference for calibration. All of the tested sensors including the proposed design, the reference design, and the commercial reference were measured by the same high-gain sensing circuit.

Fig. 6 illustrates the test setup. The sensor is placed in the vacuum chamber with Zinc Selenide (ZnSe) window. Note that ZnSe is the most popular window material for its low absorptivity at infrared wavelengths and its visible transmission. The black-body radiator emit radiation toward the vacuum chamber. Finally, the sensor performance is characterized at different working pressure. The thermoelectric infrared sensor could absorb heat radiation and then transfer into voltage output. In this study, the output voltage is approximately tens to hundreds of microvolt according to the radiation. With known circuit gain, field of view, and heat flux density, the responsivity R_s which represents the efficiency of optical sensors (i.e. transfer optical energy into electrical energy) is thus determined by measuring the output voltage at a given radiation power.

Measurements in Fig. 7a depict the variation of responsivity R_s for the two designs in Fig. 1 as working pressure varying from 1atm to 25mtorr. Thus, the responsivity of infrared sensor will be decreased as the chamber pressure is increased. It indicates that the thermal

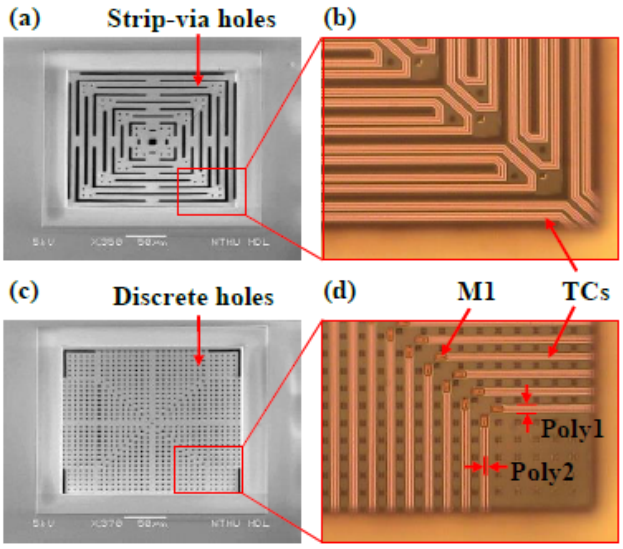

Figure 4: The SEM and OM micrographs of typical fabrication results, (a-b) the membrane and TCs of proposed design, and (c-d) the reference design.

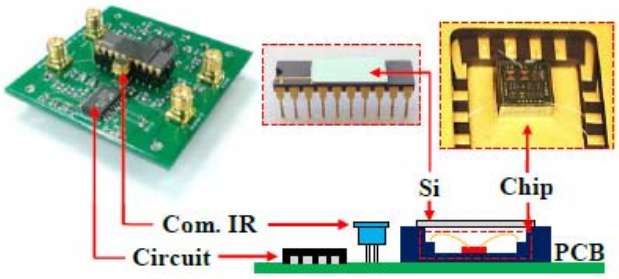

Figure 5: In-house assembly of chips on PCB for testing.

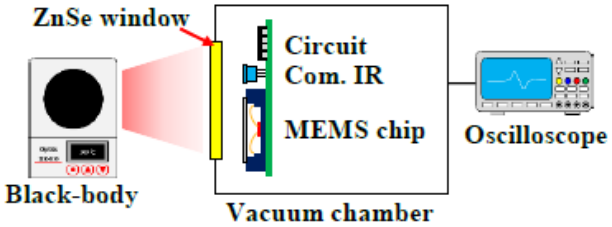

Figure 6: Measurement setup to characterize the variation of responsivity with pressure.

conduction occurs not only through the serpentine structure but also through the air between the strip-via gaps. As discussed in Fig. 2, a higher temperature difference ΔT of the TC has larger electrical output. Therefore, the proposed TC design has much better performance when lowering the thermal conduction of air. The responsivity of proposed design increases from 8.3VW^{-1} (1atm) to 146.4VW^{-1} (25mtorr) whereas the reference design increases from 14.1VW^{-1} to 23.5VW^{-1}. It shows the presented design could increase the responsivity for 6-fold
at 25mtorr working pressure. Fig. 7b further shows the normalized responsivity ($R_s/R_{s\text{-}25mtorr}$) versus pressure

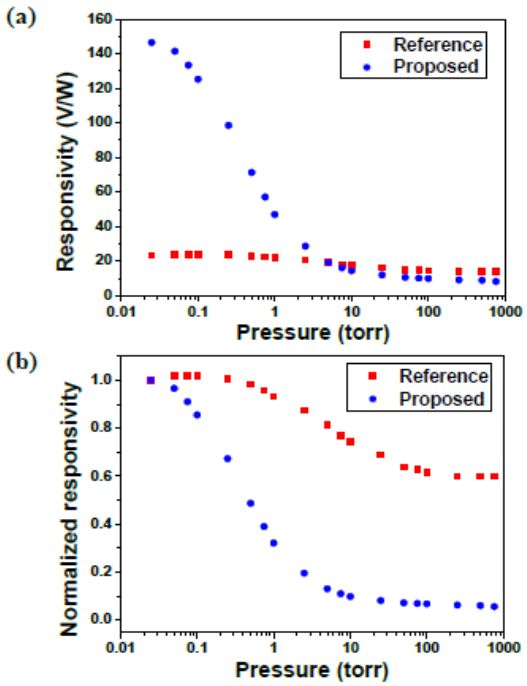

Figure 7: Responsivity vs pressure tests, (a-b) results for proposed and reference designs.

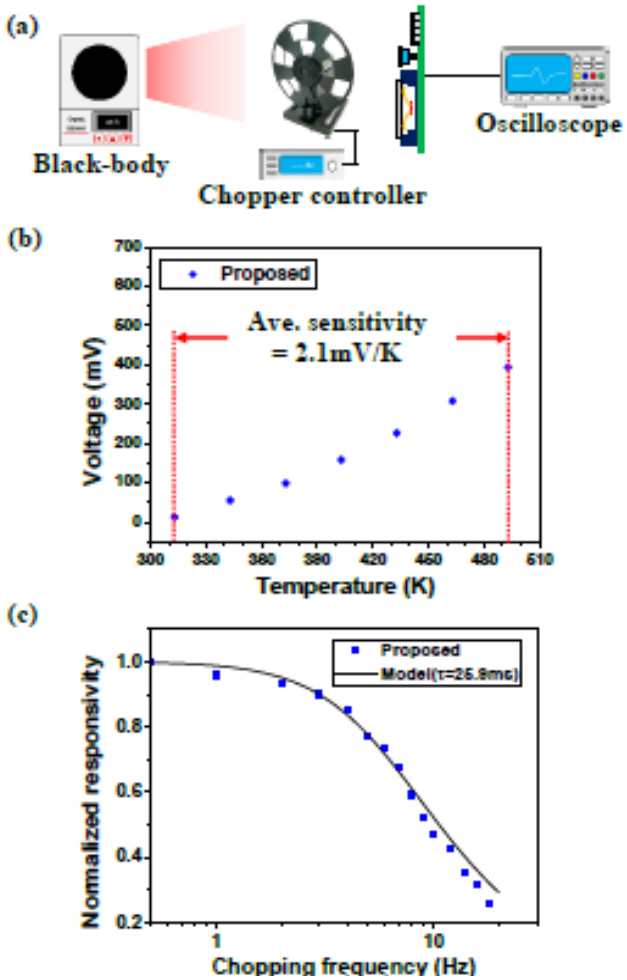

Figure 8: (a) Test setup for sensor output and response time, (b) output voltage versus object temperature at 1atm, (c) responsivity versus chopping frequency.

for these two designs. The results indicate that the influence of ambient pressure is different with the designs of absorber membrane.

Fig. 8a shows the test setup for the measurement of output voltage and the response time. Fig. 8b shows the output voltage varying with the radiating temperature at 1atm and the average sensitivity is 2.1mV/K (with circuit gain). Measurements in Fig. 8c show the variation of the responsivity with the chopping frequency f_{ch}. As the normalized responsivity dropped to the value of 0.707, the equivalent thermal time constant τ can then be extracted from the following equation [4],

$$\tau = 1/(2\pi f_{ch}) \qquad (1)$$

Thus, the equivalent thermal time constant is determined as τ = 25.9ms. After that, the variation of the normalized responsivity $R_s/R_{s\text{-}25mtorr}$ with the chopping frequency f_{ch} can be predicted from the following equation [4],

$$\frac{R_s}{R_{s-25mtorr}} = \frac{1}{\sqrt{1+4(\pi f_{ch})^2\tau^2}} \qquad (2)$$

As indicated in Fig. 8c, the results predicted by the model fit well with the measurements.

CONCLUSION

In this study, a CMOS-MEMS thermoelectric infrared sensor is successfully fabricated and demonstrated with the feature of novel absorber membrane to enhance the responsivity at low working pressure compare to the reference design in the same dimension and nearly the same noise level. As the ambient pressure decreased from 1 atm to 25mtorr, the responsivity of proposed design drastically increases from 8.3VW^{-1} (1atm) to 146.4VW^{-1} (25mtorr) whereas the reference design increases from 14.1VW^{-1} (1atm) to 23.5VW^{-1} (25mtorr). The detectivity of proposed and reference designs at 25 mtorr are 0.29×10^8 $cmHz^{0.5}W^{-1}$ and 0.05×10^8 $cmHz^{0.5}W^{-1}$, respectively. The specifications of these two designs are summarized at Table 1.

Table 1: Specification of two designs

	Reference	**Proposed**	Unit
Size	210x210	210x210	μm
Fill factor	92.1%	84.2%	
No. of junctions	80	16	
Responsivity (1atm)	14.1	8.3	VW^{-1}
Responsivity (25mtorr)	23.5	146.4	VW^{-1}
Detectivity (1atm)	0.03	0.02	$10^8cmHz^{0.5}W^{-1}$
Detectivity (25mtorr)	0.05	0.29	$10^8cmHz^{0.5}W^{-1}$

ACKNOWLEDGMENT

This project was support by the ministry of science and technology of Taiwan under grant number MOST 104-2221-E-007 -016 -MY3, MOST 105-2221-E-007 -026 -MY3, and MOST 105-2622-8-007 -006 -TE3. The authors are grateful to the TSMC and the National Chip Implementation Center, Taiwan, for supporting IC manufacturing. The authors are also grateful to the Center for Nanotechnology, Materials Science, and Microsystems at the National Tsing Hua University, National Nano Device Laboratories, Taiwan, and PixArt Imaging Incorporation, Taiwan, for providing the fabrication and measurement facilities.

REFERENCES

[1] A. Rogalski, *Progress in quantum electronics,* vol 27, pp. 59-210, 2003.

[2] E. Socher et al., *J. of Micromechanics and Microengineering,* vol 11, pp. 574-576, 2001.

[3] H. Zhou et al.," *IEEE 26th Int. Conf. on Micro Electro Mechanical Systems,* Taipei, Taiwan, Jan., 2013, pp. 429-432.

[4] M. J. Modarres-Zadeh et al., *J. of Micromechanics and Microengineering,* vol 24, pp. 125013, 2014.

[5] D. Xu et al., *J. of Micromechanics and Microengineering,* vol 19, pp. 125003, 2009.

[6] C.-N. Chen et al., *IEEE Electron Device Letters*, vol 32, pp. 96-98, 2011.

[7] J. Tanaka et al., *IEEE 27th Int. Conf. on Micro Electro Mechanical Systems*, San Francisco, CA, Jan., 2014, pp. 1213-1216.

CONTACT

* Weileun Fang; fang@pme.nthu.edu.tw